ARTICLES

Femtosecond UV Pump/Near-IR Probe Studies of the Solvent-Dependent Excited-State Decay Dynamics of Chlorine Dioxide

Sophia C. Hayes, Catherine C. Cooksey, Paul M. Wallace, and Philip J. Reid*

Department of Chemistry, University of Washington, Box 351700, Seattle, Washington 98195

Received: May 14, 2001; In Final Form: July 2, 2001

The excited-state decay and geminate-recombination dynamics of chlorine dioxide (OClO) are investigated using UV pump/near-IR probe spectroscopy. Experiments are performed with 200-fs time resolution on OClO dissolved in water, cyclohexane, acetonitrile, and chloroform. In all solvents, a reduction in optical density is observed at early times and is attributed to stimulated emission from the optically prepared $^2A_2$ surface. The emission decays on the subpicosecond time scale to reveal an increase in optical density corresponding to the production of vibrationally hot ground-state OClO formed by geminate recombination of the primary photoproducts. Kinetic analysis of these data reveals that the excited-state decay time constant increases from ~200 fs in water and cyclohexane to ~400 fs in acetonitrile and chloroform. The vibrational-relaxation dynamics of OClO are also found to be solvent dependent in agreement with earlier work. Pump–probe anisotropy experiments on aqueous OClO are presented. In these studies, an initial anisotropy of 0.40 ± 0.05 is observed consistent with emission from the optically prepared $^2A_2$ state. However, the optical-density evolution for vibrationally hot OClO displays an anisotropy of 0.08 ± 0.03 suggesting that the mechanism of geminate recombination results in the retention of memory regarding the photoexcitation event. Potential recombination mechanisms consistent with this result are discussed.

Introduction

Defining how solvents influence excited-state relaxation and geminate-recombination dynamics is central to understanding chemical reactivity in condensed media.[1–3] Attempts to achieve this understanding have focused on the dynamics of diatomic solutes.[3–18] These studies have shown that in general, photo-initiated dissociation is followed by subpicosecond geminate recombination of the nascent photofragments resulting in the reformation of the parent species. The initial excess vibrational energy created by recombination is lost to the solvent through intermolecular vibrational relaxation, and both collisional and dielectric processes have been shown to be important in defining the vibrational-relaxation rate.[1,3,12–14,19–21] Subpicosecond photo-fragment recombination has been observed in a variety of solvents suggesting that the primary recombination rate is relatively insensitive to the details of the solvent.[3,22] However, the efficiency of recombination is solvent dependent.[3,14]

There has been a great deal of interest in determining if the pattern of reactivity demonstrated by diatomic systems is also observed for triatomics. For example, in contrast to the rapid recombination seen for many diatomics, slow geminate recombination (3.5 ps) is observed for aqueous O_3^- with this behavior attributed to strong electrostatic interactions between the photofragments and the solvent.[23] Studies of I_3^- dissolved in cooled and glassy ethanol have shown that the quantum yield for geminate recombination increases with a reduction in temper-

ature consistent with increased rigidity of the solvent shell.[24] Finally, studies of aqueous CS_2 have demonstrated efficient geminate recombination of the CS and S photofragments and have assigned this behavior to solvent-assisted excited-state internal conversion.[25]

Chlorine dioxide (OClO) represents an excellent opportunity to extend our current understanding of triatomic reactivity in condensed media. This compound is of practical interest because of its involvement in a variety of stratospheric photochemical processes.[26] Photoexcitation resonant with the $^2B_1$–$^2A_2$ electronic transition results in population of the $^2A_2$ state, with excitation energies greater than 3.1 eV resulting in direct dissociation from this surface.[27,28] With lower-energy excitation, the $^2A_2$ state demonstrates predissociative behavior, and internal conversion to the nearby $^2A_1$ state followed by internal conversion from this state to the $^2B_2$ surface provides for photoproduct production.[26] Gas-phase experiments have demonstrated that of the two photoproduct channels, ClO/O and Cl/O_2, the ClO and O channel is dominant.[27] Femtosecond photofragmentation studies of gaseous OClO have investigated the time scale over which the above dynamics occur and have found that direct dissociation produced ClO and O with a 40 fs time constant, while coupling of the $^2A_2$ state with nearby surfaces produced ClO and O and Cl and O_2 with a time constant of 300 fs.[29]

In condensed environments, the reaction dynamics become more complex. In particular, the quantum yield for Cl production increases from <0.04 in the gas phase to 0.1 in solution.[27,28,30–35] The partitioning between photoproduct channels is solvent-

* To whom correspondence should be addressed. E-mail: preid@chem.washington.edu.

dependent, and recent femtosecond pump—probe and time-resolved resonance Raman (TRRR) studies have been performed to elucidate the details behind this behavior.[30-42] These experiments have shown that in solution, the dynamics are dominated by subpicosecond geminate recombination of the ClO and O photoproducts resulting in the reformation of vibrationally excited ground-state OClO. In addition, Cl formation occurs through a bifurcated process with the 'prompt' production of Cl accompanied by additional production on the ~200 ps time scale via decomposition of ground-state ClOO.[27,32] Comparative studies in water and acetonitrile have shown that both the geminate-recombination quantum yield and the OClO vibrational-relaxation rate are substantially reduced in acetonitrile relative to water.[38-42] Although a detailed description of OClO photochemistry in the condensed phase has begun to emerge, the steps leading to dissociation and photofragment recombination remain unclear. For example, photoproduct formation is initiated by decay of the optically prepared $^2A_2$ state; however, the lifetime of this state in solution has not been definitely measured. Also, the geminate-recombination dynamics resulting in ground-state OClO reformation, including the role of solvent in defining these dynamics, are unclear.

Here, we report the results of femtosecond UV pump/near-IR probe studies designed to monitor the early-time reaction dynamics of OClO. This work complements our earlier pump—probe studies which found that the production of ground-state OClO was solvent-dependent; however, the time scale for excited-state decay or the appearance of ground-state OClO could not be determined because of the limited probe wavelengths and time resolution employed. In this study, the evolution in optical density following OClO photoexcitation at 390 nm is monitored using probe wavelengths at 1210, 1270, and 1350 nm. These probe wavelengths are ideally suited to study both the decay of the optically prepared excited state as well as geminate recombination of the primary photoproducts. Experiments are performed in water and acetonitrile in an attempt to connect with our earlier work; however, two additional solvents are also investigated: cyclohexane and chloroform. Cyclohexane is employed to investigate how the photochemistry of OClO proceeds in nonpolar environments. Chloroform is included to compare the dynamics that occur in this polar aprotic solvent to those that occur in acetonitrile. In addition, we are interested in connecting the results of this study to recent resonance Raman intensity analysis work of OClO in chloroform.[43] Two main conclusions regarding OClO photochemistry are derived in this study. First, the decay of the optically prepared excited state is found to be solvent-dependent, with decay time constants ranging from ~200 fs in water and cyclohexane to ~400 fs in acetonitrile and chloroform. It is proposed that solvent dependence of the $^2A_2$ and $^2A_1$ state energetics is responsible for the solvent dependence of the exited-state decay rate. Second, femtosecond pump—probe anisotropy experiments are presented which demonstrate that memory of the photoexcitation event is maintained through the geminate-recombination process. Potential mechanisms involving incomplete rotational diffusion of the nascent photofragments and solvent-dependent internal conversion dynamics are presented that are consistent with this result. In summary, the results presented here provide new insight into the solvent-dependent excited-state relaxation and geminate-recombination dynamics of OClO.

Materials and Methods

The laser system employed in this work is similar to that used in previous studies;[38-41] therefore, only a brief description
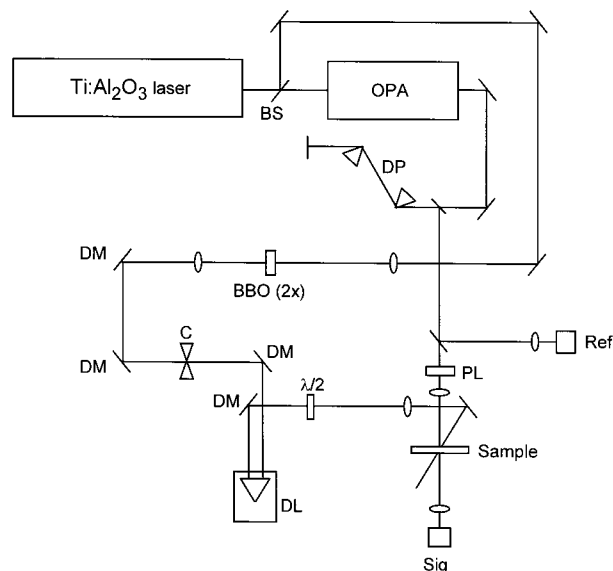

Figure 1. Schematic of the pump—probe spectrometer. The following abbreviations have been used: BBO (2x): frequency doubling β-barium borate crystal; BS: Beam splitter; C: mechanical chopper; DL: optical-delay line; DM: dichroic mirror; DP: Brewster dispersion prisms; $\lambda/2$: zero-order half-wave plate; OPA: optical parametric amplifier; PL: calcite polarizer.

is provided here. An argon-ion laser (Spectra Physics 2065—07) operating all-lines pumped a home-built Ti:Sapphire oscillator that produced 30-fs pulses (full-width at half-maximum or fwhm) centered at 780 nm at a repetition rate of 91 MHz. Amplification of these pulses was performed using the chirped-pulse technique[44] (Clark-MXR CPA-1000-PS). The post-compression amplified output consisted of 85-fs fwhm pulses centered at 780 nm with pulse energy of 700 μJ at a repetition rate of 1 kHz. The amplifier output was split into two components, with 20% of the output frequency doubled using a 200-μm thick β-BBO (Type I) crystal to generate the actinic field. The remainder of the amplifier output was used to pump an optical parametric amplifier (OPA, Quantronix TOPAS), with the signal output used as the probe.

The optical layout employed in this study is presented in Figure 1. Pre-compensation for group-velocity dispersion of the probe field was provided by a pair of SF-10 prisms. A Glan-Laser calcite polarizer was placed in the probe line following the prism pair to define the probe polarization. The pump beam was temporally adjusted relative to the probe using a motorized delay stage. The contribution of rotation dynamics to the data was minimized by orientation of the pump polarization to 54.7° relative to the probe using a zero-order half-wave plate. Time-resolved absorption anisotropy experiments were performed at 1270 nm. In these studies, the pump polarization was rotated to be aligned ($I_{\parallel}$) or orthogonal ($I_{\perp}$) to that of the probe. The time-dependent absorption anisotropy ($r(t)$) was then constructed from these data according to

$$r(t) = \frac{I_{\parallel} - I_{\perp}}{I_{\parallel} + 2I_{\perp}}$$

In all experiments, the instrument response as measured by difference-frequency generation using a 200-μm thick β-BBO crystal (type II) was 200 ± 20 fs (fwhm).

OClO was synthesized as previously described.[44] All solvents were HPLC grade and used without further purification. The pump and probe powers were adjusted using reflective, fused-silica neutral density filters. Typical pulse energies were 4.0 ±
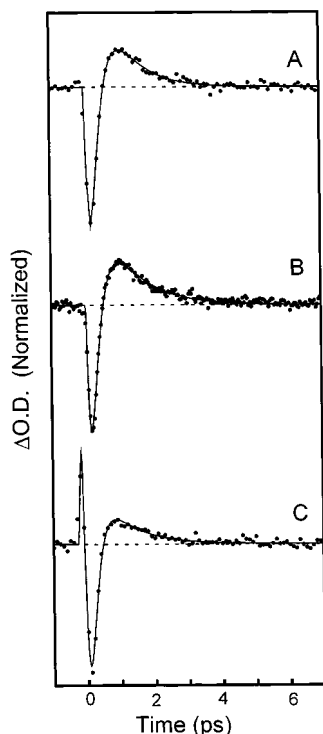
Femtosecond UV Pump/Near-IR Probe Studies

J. Phys. Chem. A, Vol. 105, No. 43, 2001 **9821**

Figure 2. Time-resolved pump−probe dynamics of aqueous OClO with photoexcitation at 390 nm and probe wavelengths of **(A)** 1210, **(B)** 1270, and **(C)** 1350 nm. Best fit to the data by a sum of three exponentials convolved with the instrument response is given by the solid line, with corresponding fit parameters presented in Table 1.

0.5 μJ and 0.1 $\pm$ 0.05 μJ for the pump and probe, respectively. The spot-size of the pump and the probe at the sample were 550 and 500 μm, respectively. Samples were delivered to a fused-silica flow cell, and the flow rate was adjusted to ensure that the sample volume was replenished between actinic events. Detection of the pump-induced change in optical density was performed as described elsewhere,[40] with the exception that the sample and reference probe signals were detected using InGaAs photodiodes (Fermionics FD3000W). The time-dependent evolution in optical density was analyzed by fitting the data to a convolution of the instrument response with a sum of three exponentials using the Levenberg−Marquardt algorithm.[46] Goodness of fit was judged through χ^2 values as well as visual inspection of the residuals. Reported errors correspond to one standard deviation from the mean determined by multiple measurements (≥ 5 trials). The data were also analyzed by comparison to a kinetic model as described below. In this work, the differential rate expressions corresponding to the model were evaluated using Euler's method employing a 2.5-fs step size. Further reduction in the step size did not affect the results presented here.

Results

Femtosecond Pump−Probe Studies. Figure 2 presents the evolution in optical density observed for aqueous OClO at 1210, 1270, and 1350 nm following photoexcitation at 390 nm. At all probe wavelengths, a pump-induced reduction in optical density is observed. Absorption corresponding to the $^2B_1-^2A_2$ transition is negligible in this wavelength region such that the reduction in optical density cannot be assigned to ground-state depletion via photolysis. Instead, we assign this feature to stimulated emission from the optically prepared $^2A_2$ surface. Support for this assignment is found in the time-resolved absorption anisotropy data where an initial anisotropy of 0.40

$\pm$ 0.05 is observed consistent with emission from a single, dipole allowed electronic transition (see below). Furthermore, recent studies of OClO fluorescence in condensed environments have demonstrated that the fluorescence undergoes a substantial Stokes shift providing for emission in the near-IR.[43,47] Following decay of the stimulated emission, an increase in optical density is observed (Figure 2). In previous pump−probe studies, increases in optical density were observed for probe wavelengths out to 1000 nm and were assigned to vibrationally excited ground-state OClO produced by geminate recombination of the primary photofragments.[33,34] Consistent with this interpretation, we assign the later-time appearance and decay of optical density to the production and vibrational relaxation of ground, $^2B_1$-surface OClO.

An initial analysis was performed which involved fitting these data to a sum of three exponentials convolved with the instrument response. The results of this analysis for all probe wavelengths employed are presented in Table 1, and the corresponding fits are shown as the solid lines in Figure 2. At 1270 nm in water, the stimulated emission appears and decays with time-constants of 80 $\pm$ 40 ps and 200 $\pm$ 30 fs, respectively. In addition, aqueous OClO undergoes vibrational relaxation with an apparent time constant of 1.20 $\pm$ 0.43 ps, in excellent agreement with previous pump−probe results.[34,35,40,41] The time constants observed at the other probe wavelengths are equivalent to those observed at 1270 nm within the experimental error such that probe wavelength dependence of the kinetics is minimal. A sharp increase in optical density is observed at 1350 nm in water necessitating the addition of a fourth exponential to accurately reproduce the data (τ_4 in Table 1). This increase in optical density most likely originates from an overtone transition of the solvent, with the 1350 nm probe wavelength being on the blue-edge of this absorption. In the other solvents studied, significant solvent absorbance is not present in this wavelength region, and a corresponding optical density increase at early times was not observed. Attempts to employ longer probe wavelengths were frustrated by the finite absorbance of the solvents that rendered the sample opaque in the near-IR.

Figure 3 presents a comparison of the optical density evolution for OClO dissolved in water, cyclohexane, acetonitrile, and chloroform at 1270 nm. Contrary to other work, stimulated emission is observed in all the solvents employed in this study.[42] The figure demonstrates that the magnitude of the stimulated emission is similar in all solvents; however, the time scale for stimulated emission decay is solvent-dependent. Emission decay appears to be most rapid in water and slowest in acetonitrile or chloroform. In addition, the OClO vibrational-relaxation kinetics appears to be faster in water relative to acetonitrile and chloroform reminiscent of the behavior observed in earlier studies.[40] Identical to the approach described above, the time-dependent optical density evolution in all solvents was fit to a sum of exponentials convolved with the instrument response. The results of this analysis are presented in Table 1. The table demonstrates that at 1270 nm, the stimulated emission appearance time constant (τ_1) is essentially solvent-invariant. However, the apparent stimulated emission decay time constant (τ_2) is strongly solvent-dependent, increasing from 200 $\pm$ 30 fs in water to 930 $\pm$ 80 fs in acetonitrile. Finally, the vibrational-relaxation time constant for ground-state OClO undergoes a substantial increase from 1.20 $\pm$ 0.43 ps in water to 8.0 $\pm$ 1.5 ps in chloroform. Similar behavior is observed at other probe wavelengths as reported in Table 1.

Kinetic Analysis. In addition to the fitting procedure presented above, we also employed a kinetic model to assist in

TABLE 1: Fit Parameters Determined from Analysis of the Pump−Probe Data

	$A_1{}^a$	τ_1 (ps)	A_2	τ_2 (ps)	A_3	τ_3 (ps)	A_4	τ_4 (ps)
				Water				
1210 nm[b]	$0.36 \pm 0.09{}^c$	0.13 ± 0.04	-0.52 ± 0.02	0.25 ± 0.05	0.12 ± 0.09	1.0 ± 0.5		
1270 nm	0.47 ± 0.24	0.08 ± 0.04	-0.46 ± 0.21	0.20 ± 0.03	0.06 ± 0.03	1.2 ± 0.4		
1350 nm	0.49 ± 0.07	0.09 ± 0.02	-0.16 ± 0.09	0.24 ± 0.04	0.02 ± 0.01	0.9 ± 0.3	0.07 ± 0.02	0.32 ± 0.15
				Cyclohexane				
1210 nm	0.68 ± 0.21	0.05 ± 0.04	-0.27 ± 0.17	0.69 ± 0.13	0.05 ± 0.04	4.8 ± 1.8		
1270 nm	0.39 ± 0.14	0.11 ± 0.04	-0.52 ± 0.11	0.49 ± 0.12	0.09 ± 0.04	4.7 ± 0.8		
1350 nm	0.35 ± 0.08	0.10 ± 0.04	-0.56 ± 0.04	0.48 ± 0.10	0.09 ± 0.05	4.9 ± 1.3		
				Acetonitrile				
1210 nm	0.38 ± 0.28	0.05 ± 0.03	-0.51 ± 0.22	1.15 ± 0.16	0.11 ± 0.07	5.9 ± 2.3		
1270 nm	0.33 ± 0.15	0.11 ± 0.05	-0.61 ± 0.15	0.93 ± 0.08	0.07 ± 0.04	6.1 ± 2.3		
1350 nm	0.41 ± 0.15	0.19 ± 0.12	-0.48 ± 0.09	0.92 ± 0.20	0.11 ± 0.09	5.6 ± 3.9		
				Chloroform				
1210 nm	0.38 ± 0.06	0.15 ± 0.06	-0.50 ± 0.03	1.20 ± 0.11	0.13 ± 0.04	5.7 ± 2.0		
1270 nm	0.55 ± 0.11	0.11 ± 0.05	-0.40 ± 0.10	0.79 ± 0.10	0.05 ± 0.01	8.0 ± 1.5		
1350 nm	0.47 ± 0.05	0.07 ± 0.02	-0.44 ± 0.05	0.68 ± 0.24	0.10 ± 0.07	9.2 ± 3.5		

[a] Amplitudes are normalized such that $\Sigma|A_i| = 1$. [b] Entries refer to probe wavelength. [c] Errors represent one standard deviation from the mean for all measurements at a given probe wavelength.
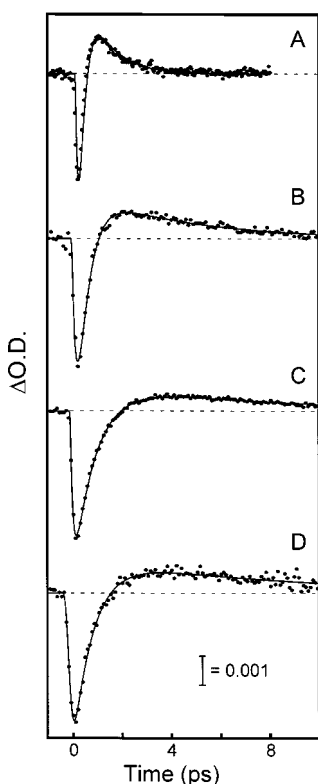

Figure 3. Time-resolved pump−probe dynamics of OClO dissolved in **(A)** water, **(B)** cyclohexane, **(C)** acetonitrile, and **(D)** chloroform, with pump and probe wavelengths of 390 and 1270 nm, respectively. Best fit to the data by a sum of three exponentials convolved with the instrument response is given by the solid line, with the corresponding fit parameters presented in Table 1.
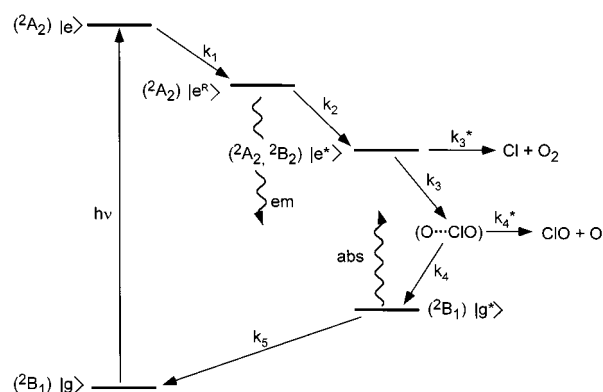

Figure 4. Proposed kinetic scheme for OClO. Photoexcitation ($h\nu$) leads to production of the optically prepared excited state ($|e\rangle$) with vibrational relaxation (k_1) resulting in population of the relaxed excited state ($|e^R\rangle$). Internal conversion from the relaxed excited state (k_2) results in the population of an optically dark excited state ($|e^*\rangle$). Decay of the optically dark state results either in the production of photoproducts Cl + O$_2$ with rate $k_3{}^*$ or in the formation of a distorted intermediate (O···ClO) with rate k_3. This intermediate either decays with rate k_4 to reform vibrationally excited ground-state OClO ($|g^*\rangle$), which undergoes subsequent vibrational relaxation (k_5), or it dissociates to the photoproducts ClO + O with rate $k_4{}^*$. The wavy arrows indicate the surfaces from which the observed transient emission and absorption originate.

the interpretation of the optical density evolution. The model is presented in Figure 4 and has as its origin a similar model proposed by Zewail and co-workers for gaseous OClO.[29] The kinetic scheme is based on the following sequence of events. Photoexcitation of ground-state OClO ($|g\rangle$) results in population of vibronic levels of the $^2A_2$ state ($|e\rangle$) that are Franck−Condon coupled to the optical transition. Both intramolecular and intermolecular vibrational relaxation provide for population of lower-energy levels of the $^2A_2$ surface ($|e^R\rangle$) from which stimulated emission occurs. These vibrational-relaxation processes are represented by the rate constant k_1. Internal conversion from the $^2A_2$ surface results in population of the $^2A_1$ state, with

subsequent internal conversion from this surface leading to population of the $^2B_2$ surface.[26,48] Internal conversion from the relaxed levels of the $^2A_2$ surface is represented by the rate constant k_2. The transition moments between the $^2A_1$ or $^2B_2$ surface and the ground state are weak; therefore, stimulated emission from these surfaces is not considered. In addition, the limited optical activity of these surfaces prohibits a separate investigation of the $^2A_1$ state decay; therefore, the populations on these two surfaces are treated as a single, composite population ($|e^*\rangle$). Decay of the $^2A_1$ and $^2B_2$ surfaces results either in the production of Cl and O$_2$ with rate constant $k_3{}^*$ or in the production of a distorted intermediate (O···ClO) with rate constant k_3. This intermediate is a precursor to both vibrationally excited ground-state OClO ($|g^*\rangle$) and the photoproducts ClO and O. The production of these photoproducts is modeled by the rate constants k_4 and $k_4{}^*$, respectively. Finally, vibrational relaxation of ground-state OClO is modeled through the rate constant k_5.

Two major assumptions have been made in constructing the kinetic model. First, decay of the $^2A_2$ surface only occurs

Femtosecond UV Pump/Near-IR Probe Studies

J. Phys. Chem. A, Vol. 105, No. 43, 2001 **9823**

through internal conversion in this model; however, direct dissociation from this surface is known to occur.[29,34,49] The extent of direct dissociation depends on actinic wavelength, with the wavelength used here providing for only limited dissociation ($\leq 5\%$).[34] Second, it is known that photoproduct formation is a bifurcated process with the production of atomic chlorine occurring via two distinct mechanisms.[32,37] Such effects could be incorporated into the kinetic scheme through the separation of k_3^* into individual components; however, this modification would necessitate the inclusion of more undefined parameters and was judged as unwarranted at present.

The model presented here can also be viewed as a modified version of an early model presented by Keiding and co-workers that was developed to interpret the optical density evolution for aqueous OClO at 260, 390, and 780 nm.[35] The mechanism proposed by these authors considered evolution following $^2B_2$ state production. Two photoproduct channels were then accessed from this state, one leading to formation of Cl and O_2 via an unidentified intermediate species and the other leading to formation of ClO and O which recombine to produce vibrationally excited ground-state OClO. Besides the addition of the early-time dynamics on the $^2A_2$ surface, we have extended this earlier model by including the possibility of cage escape of the ClO and O photofragments via the step with rate constant k_4^*. As will be discussed below, the rate constants found here for aqueous OClO are in good agreement with the results reported by Keiding and co-workers.

The kinetic scheme presented in Figure 4 was employed to reproduce the optical density evolution observed following OClO photoexcitation. The optical-density evolution presented in Figures 2 and 3 suggests that two contributions are dominant, emission from the relaxed levels of the $^2A_2$ surface and absorption of vibrationally excited ground-state OClO, as indicated by the wavy arrows in Figure 4. Consistent with this observation, the optical-density evolution was modeled by the following:

$$\Delta O.D. = \int G(t'-t)(-A_{em}[e^R(t)] + A_{abs}[g^*(t)])dt$$

where A_{em} and A_{abs} are the stimulated emission and absorption amplitudes, and $[e^R(t)]$ and $[g^*(t)]$ are the time-dependent concentrations of the relaxed excited state and vibrationally excited ground-state OClO, respectively. The predicted evolution in optical density arising from these two species was convolved with the instrument response ($G(t)$) for comparison to experiment. In performing this analysis, results from previous pump–probe studies were used to constrain a subset of the rate constants. Specifically, the ground-state vibrational-relaxation rate constant (k_5) in water and acetonitrile was fixed to previously determined values.[34,40] In addition, the geminate-recombination quantum yields in water (0.80 ± 0.05),[34,38,40] cyclohexane (0.50 ± 0.05),[42,50] acetonitrile (0.33 ± 0.1),[40] and chloroform (0.26 ± 0.1)[50] were used to constrain the relative values of k_4 and k_4^*. The quantum yield for Cl production (0.07 ± 0.03), as defined by previous pump–probe studies,[30–35] was assumed to be the same in all solvents and was used to constrain the values of k_3 and k_3^*. The rate constant for ClO production (k_3) was constrained by previous pump–probe results for OClO dissolved in water and acetonitrile measured at 260 nm.[40] Finally, the stimulated emission amplitude was constrained to be identical in all solvents.

Figure 5 presents a comparison between the measured evolution in optical density for OClO dissolved in cyclohexane and that predicted using the kinetic model. Inspection of the
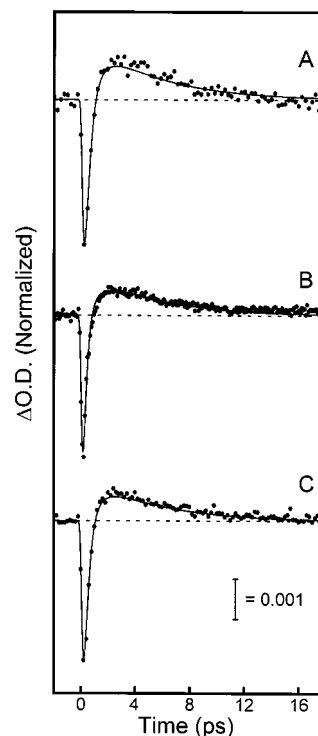

Figure 5. Time-resolved pump–probe dynamics of OClO dissolved in cyclohexane with photoexcitation at 390 nm and probe wavelengths of (**A**) 1210, (**B**) 1270, and (**C**) 1350 nm. The solid lines represent the best fit to the data using the kinetic scheme presented in Figure 4 as described in the text. Parameters corresponding to the fit are given in Table 2.

TABLE 2: Kinetic Parameters Determined from Analysis of the Pump–Probe Data

	τ_1 (ps)[a]	τ_2 (ps)	τ_3 (ps)	τ_3^* (ps)	τ_4 (ps)	τ_4^* (ps)	τ_5 (ps)	A_{em}[b]	A_{abs}[b]	$\phi_{g.r.}$[c]
				Water						
1210 nm[d]	0.09	0.16	0.4	4.0	0.15	1.2	0.7	0.0095	0.003	0.81
1270 nm	0.08	0.14	0.4	4.0	0.14	1.2	0.8	0.0095	0.003	0.82
1350 nm	0.08	0.13	0.3	3.0	0.15	1.2	0.8	0.0095	0.0017	0.81
				Cyclohexane						
1210 nm	0.22	0.27	1.0	10	0.20	0.18	5.0	0.0095	0.003	0.43
1270 nm	0.15	0.19	1.0	10	0.27	0.15	5.0	0.0095	0.003	0.33
1350 nm	0.21	0.24	1.0	10	0.20	0.18	5.0	0.0095	0.0022	0.43
				Acetonitrile						
1210 nm	0.38	0.45	2.3	23.0	0.20	0.11	5.0	0.0095	0.003	0.33
1270 nm	0.35	0.37	2.8	23.0	0.20	0.11	4.3	0.0095	0.003	0.32
1350 nm	0.37	0.37	2.4	24.0	0.15	0.10	4.3	0.0095	0.0017	0.37
				Chloroform						
1210 nm	0.37	0.40	1.8	18.0	0.25	0.10	7.0	0.0095	0.003	0.26
1270 nm	0.30	0.33	1.8	18.0	0.25	0.10	7.0	0.0095	0.003	0.26
1350 nm	0.22	0.25	1.9	19.0	0.25	0.10	7.0	0.0095	0.0019	0.26

[a] Time constants that are equivalent to $1/k$ with k being the microscopic rate constant as illustrated in Figure 4. [b] Amplitudes for the excited-state emission (em) and the absorption (abs) of vibrationally unrelaxed ground-state OClO. [c] The geminate-recombination quantum yield. [d] Entries refer to probe wavelength.

figure demonstrates that the model accurately reproduces the evolution in optical density. Similar agreement was found for water, acetonitrile, and chloroform (comparison not shown). The kinetic parameters determined from this analysis are presented in Table 2. Inspection of these parameters demonstrates that many of the kinetic steps are solvent-dependent. For example, the internal conversion time constant (τ_2) increases from ~150 fs in water or ~230 fs in cyclohexane to ~400 fs in acetonitrile and chloroform demonstrating that internal conversion from the
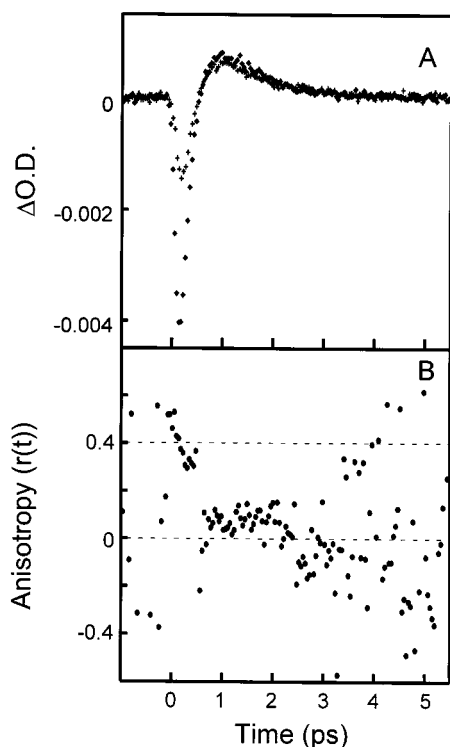
9824 *J. Phys. Chem. A, Vol. 105, No. 43, 2001*

Hayes et al.

Figure 6. (A) Polarization-dependent pump−probe dynamics for aqueous OClO. Data were obtained with pump and probe wavelengths of 390 and 1270 nm, respectively. The diamonds and crosses represent the data obtained with parallel and perpendicular pump and probe polarizations, respectively. (B) The time-dependent anisotropy derived from the data presented in (A) as described in the text.

$^2A_2$ state is solvent-dependent. In addition, the time constant for formation of the asymmetric intermediate (τ_3) increases from ∼400 fs in water to ∼2.5 ps in acetonitrile, in agreement with our previous pump−probe work and the kinetic model proposed by Keiding and co-workers for aqueous OClO.[35,40] The production of Cl appears to be solvent-dependent with time constants τ_3^* ranging from 4 ps in water to 24 ps in acetonitrile. The value for water reported here is identical to that reported by Keiding and co-workers.[35] Finally, the time constant for OClO production (τ_4) is very similar in all solvents consistent with the rate of geminate recombination being insensitive to the details of the solvent.[38]

Pump−Probe Anisotropy. The analysis presented above assumes that the reduction in optical density at early times is due to stimulated emission from the $^2A_2$ surface. Pump−probe anisotropy measurements were performed to test this assumption. Figure 6A presents the polarization-dependent optical-density evolution for aqueous OClO with pump and probe wavelengths of 390 and 1270 nm, respectively. The time-dependent anisotropy determined using these data is presented in Figure 6B. The figure demonstrates that an initial anisotropy of 0.40 ± 0.05 is observed consistent with emission originating from a single, dipole-allowed electronic transition. This initial anisotropy value supports the assignment of the early-time reduction in optical density to stimulated emission from the $^2A_2$ state. As the delay between the pump and probe increases, the initial anisotropy decays and undergoes a discontinuity at ∼800 fs as the optical-density evolution switches from emissive to absorptive. After this time, a residual anisotropy of 0.08 ± 0.03 is observed that undergoes slow decay. The absorptive signal observed at these later-time delays has been assigned to vibrationally excited ground-state OClO produced through geminate recombination.[34,35,40,41] Therefore, the observation of

a nonvanishing anisotropy for the absorptive optical-density component suggests that memory of the photoexcitation event is carried through to the production of the geminately recombined product.

Discussion

Solvent-Dependent Excited-State Dynamics. The optical-density evolution observed in these studies demonstrates that the excited-state internal conversion dynamics of OClO are solvent-dependent. The data analysis performed with the kinetic model found that the $^2A_2$ state internal-conversion rate is similar in water and cyclohexane, but is 2-fold slower in acetonitrile and chloroform (τ_2 in Table 2). As mentioned in the Introduction, the predominant decay pathway for the $^2A_2$ surface is internal conversion to the $^2A_1$ surface, and we propose that the alteration in the internal-conversion rate reflects solvent-dependence of the $^2A_2$ and $^2A_1$ state relative energies. Both resonance Raman depolarization ratio[51] and fluorescence studies[47] have shown that these two surfaces are energetically proximate. Furthermore, the resonance Raman depolarization dispersion curves for the symmetric-stretch fundamental transition in cyclohexane and water are similar consistent with the relative energetics of the $^2A_2$ and $^2A_1$ states also being similar between these solvents.[45,52] The $^2A_2$ and $^2A_1$ surfaces are coupled via a spin−orbit interaction. Assuming that the spin−orbit coupling matrix element is invariant between cyclohexane and water, we would expect the similarity in state energetics to provide for comparable internal-conversion rates. Information regarding either the fluorescence cross-section or resonance Raman depolarization ratios of OClO in acetonitrile is not available. However, recent resonance Raman intensity analysis studies have been performed on OClO dissolved in chloroform.[43] Here, the depolarization dispersion curve for the symmetric-stretch fundamental transition was significantly different from that observed in water or cyclohexane and was consistent with greater energetic separation of the $^2A_2$ and $^2A_1$ states. Given this, the reduction in internal-conversion rates in chloroform relative to water and cyclohexane is most likely due to solvent dependence of the $^2A_2$ and $^2A_1$ state energies.

The Mechanism of Ground-State OClO Production. Perhaps the most surprising result presented here is the nonvanishing anisotropy for the optical-density evolution corresponding to ground-state OClO formed by geminate recombination. This result demonstrates that at least for aqueous OClO, memory of the photoexcitation event is carried through the geminate-recombination process. If complete dissociation into ClO and O occurs, reorientation of the photofragments could result in loss of memory assuming complete reorientation of the photofragments. Therefore, the presence of residual anisotropy demonstrates that random orientation of the photofragments is not established before recombination occurs. The question remains as to the geminate-recombination dynamics that provide for retention of the memory regarding the photoexcitation event.

There are two mechanisms that are consistent with the presence of residual anisotropy: incomplete photofragment reorientation before recombination and restricted evolution along the dissociative reaction coordinate. We first consider the photofragment reorientation model. Geminate recombination is known to occur within a few hundred femtoseconds following OClO photoexcitation;[32,34,35,37−41] therefore, reorientation of the ClO and O fragments must be comparable to or slower than this time for residual anisotropy to be evident. Gas-phase studies of OClO photodissociation have demonstrated that the internal-energy content of the ClO photofragments is actinic-wavelength

Femtosecond UV Pump/Near-IR Probe Studies

J. Phys. Chem. A, Vol. 105, No. 43, 2001 **9825**

dependent.[49,53,54] However, the extent of rotational excitation is modest compared to vibrational or translational excitation. For example, photoexcitation at 351 nm results in the production of ClO with only 7% of the available excess energy into rotations providing for an effective rotational temperature of 480 ± 30 K.[49] Studies of OClO photodissociation in water clusters have shown that the ClO rotational temperature is only ~200 K. Using the rotational constant for ClO provided by Coxon (0.62 cm^{-1}),[55] this effective rotational temperature would result in a rotational correlation decay time of ~700 fs.[56] This time is comparable to the subpicosecond recombination time observed in water; therefore, the residual anisotropy may simply reflect the incomplete rotational diffusion of ClO before recombination. A critical test of this mechanism would be to perform UV pump/UV-probe experiments in which the anisotropy of optical-density changes originating from ClO are studied. Such experiments are currently underway.

A second mechanism consistent with the preservation of anisotropy after geminate recombination is that of restricted evolution along the dissociative reaction coordinate. Coker and co-workers have proposed that following I$_2$ photoexcitation, solvent-mediated fluctuations of the vibronic-state energies lead to efficient excited-state internal conversion such that evolution along the reaction coordinate is truncated before complete dissociation occurs.[9,57] If such a mechanism were operative, then the quantum yield for geminate recombination should be dependent on the efficiency of excited-state internal conversion. The kinetic analysis presented here suggests that decay times for lower-lying excited states (τ_3 and τ_3* in Table 2) are slowest in solvents where the geminate-recombination quantum yields are smallest supporting this model. In addition, the solvents investigated all demonstrate excited-state decay times that are greater than that expected for barrierless dissociation suggesting that evolution along the dissociative reaction coordinate is indeed restricted. Restricted evolution could lead to the formation of excited-state OClO that is geometrically distorted relative to the ground state. Such a species was proposed as a transition state in gas-phase studies of OClO to account for the substantial translational energy content of the Cl and O$_2$ photofragments.[26,27] The existence of a similar intermediate was also proposed in previous pump−probe studies of aqueous OClO to account for optical-density changes in the ultraviolet region of the spectrum.[35] The existence of such an intermediate hinges on the presence of a minimum on the $^2B_2$ potential-energy surface capable of supporting such a distorted structure. Ab initio studies of this surface have shown that the requisite minimum on the lower-energy $^2B_2$ surface may exist; however, the depth of this minimum is strongly dependent on symmetry.[48] Slight distortions away from C_{2v} ground-state symmetry are sufficient to significantly reduce the depth of the minimum such that the $^2B_2$ surface becomes unbound with respect to ClO and O formation.[48] Resonance Raman intensity analysis studies have shown that in solution, evolution along the asymmetric-stretch coordinate on the optically prepared excited state is dramatically reduced resulting in the preservation of C_{2v} symmetry.[43,45,51,52] Therefore, the preservation of ground-state symmetry may provide for the production of distorted OClO on the $^2B_2$ surface, with the efficiency of internal conversion from this surface dictating the extent of ground-state OClO production.

Conclusions

In this manuscript, we have presented femtosecond UV pump/ near-IR probe studies on OClO in water, acetonitrile, cyclo-hexane, and chloroform. We have observed stimulated emission

from the optically prepared $^2A_2$ state allowing for the first direct determination of the lifetime of this state in solution. Variation of the excited-state lifetime as a function of solvent was attributed to solvent dependence of the $^2A_2$ and $^2A_1$ state energetics and subsequent modification of the excited-state internal conversion rate. Pump−probe anisotropy experiments were presented that verified the assignment of the early-time optical-density evolution to stimulated emission from the $^2A_2$ state. In addition, a residual anisotropy corresponding to vibrationally excited ground-state OClO was observed, suggesting that memory of the photoexcitation event is retained through the geminate-recombination process. Two mechanisms consistent with this observation were proposed: incomplete reorientation of the nascent photofragments and restricted evolution along the dissociation coordinate. The information presented here provides a better understanding of the early-time excited-state dynamics of chlorine dioxide and the processes leading to geminate recombination of the primary photo-fragments.

References and Notes

(1) Owrutsky, J. C.; Raftery, D.; Hochstrasser, R. M. *Annu. Rev. Phys. Chem.* **1994**, *45*, 519.

(2) Laubereau, A.; Kaiser, W. *Rev. Mod. Phys.* **1978**, *50*, 607.

(3) Harris, A. L.; Brown, J. K.; Harris, C. B. *Annu. Rev. Phys. Chem.* **1988**, *39*, 341.

(4) Paige, M. E.; Harris, C. B. *Chem. Phys.* **1990**, *149*, 37.

(5) Nesbitt, D. J.; Hynes, J. T. *J. Chem. Phys.* **1982**, *77*, 2130.

(6) Xu, X.; Yu, S.-C.; Lingle, R.; Zhu, H.; Hopkins, J. B. *J. Chem. Phys.* **1991**, *95*, 2445.

(7) Lingle, R. J.; Xiaobing, X.; Soo-Chang, Y.; Huiping, Z.; Hopkins, J. B. *J. Chem. Phys.* **1990**, *93*, 5667.

(8) Cho, M.; Rosenthal, S. J.; Scherer, N. F.; Ziegler, L. D.; Fleming, G. R. *J. Chem. Phys.* **1992**, *96*, 5033.

(9) Batista, V. S.; Coker, D. F. *J. Chem. Phys.* **1996**, *105*, 4033.

(10) Zadoyan, R.; Li, Z.; Martens, C. C.; Apkarian, V. A. *J. Chem. Phys.* **1994**, *101*, 6648.

(11) Kliner, D. A. V.; Alfano, J. C.; Barbara, P. F. *J. Chem. Phys.* **1993**, *98*, 5375.

(12) Benjamin, I.; Banin, U.; Rhuman, S. *J. Chem. Phys.* **1993**, *98*, 8337.

(13) Benjamin, I.; Barbara, P. F.; Gertner, B. J.; Hynes, J. T. *J. Phys. Chem.* **1995**, *99*, 7557.

(14) Walhout, P. K.; Alfano, J. C.; Thakur, K. A. M.; Barbara, P. F. *J. Phys. Chem.* **1995**, *99*, 7568.

(15) Kuhne, T.; Vohringer, P. *J. Chem. Phys.* **1996**, *105*, 10788.

(16) Hess, S.; Bursing, H.; Vohringer, P. *J. Chem. Phys.* **1999**, *111*, 5461.

(17) Banin, U.; Waldman, A.; Ruhman, S. *J. Chem. Phys.* **1992**, *96*, 2416.

(18) Banin, U.; Ruhman, S. *J. Chem. Phys.* **1993**, *98*, 4391.

(19) Whitnell, R. M.; Wilson, K. R.; Hynes, J. T. *J. Chem. Phys.* **1992**, *96*, 5354.

(20) Hamm, P.; Lim, M.; Hochstrasser, R. M. *J. Chem. Phys.* **1997**, *107*, 10523.

(21) Heilweil, E. J.; Doany, F. E.; Moore, R.; Hochstrasser, R. M. *J. Chem. Phys.* **1982**, *76*, 5632.

(22) Schwartz, B. J.; King, J. C.; Zhang, J. Z.; Harris, C. B. *Chem. Phys. Lett.* **1993**, *203*, 503.

(23) Walhout, P. K.; Silva, C.; Barbara, P. F. *J. Phys. Chem.* **1996**, *100*, 5188.

(24) Zhaohui, W.; Wasserman, T.; Gershgoren, F.; Vala, J.; Kosloff, R.; Ruhman, S. *Chem. Phys. Lett.* **1999**, *313*, 155.

(25) Thomsen, C. L.; Madsen, D.; Thogersen, J.; Byberg, J. R.; Keiding, S. R. *J. Chem. Phys.* **1999**, *111*, 703.

(26) Vaida, V.; Simon, J. D. *Science* **1995**, *268*, 1443.

(27) Davis, H. F.; Lee, Y. T. *J. Phys. Chem.* **1992**, *96*, 5681.

(28) Davis, H. F.; Lee, Y. T. *J. Phys. Chem.* **1996**, *100*, 8142.

(29) Baumert, T.; Herek, J. L.; Zewail, A. H. *J. Chem. Phys.* **1993**, *99*, 4430.

(30) Chang, Y. J.; Simon, J. D. *J. Phys. Chem.* **1996**, *100*, 6406.

(31) Dunn, R. C.; Flanders, B. N.; Simon, J. D. *J. Phys. Chem.* **1995**, *99*, 7360.

(32) Thomsen, C. L.; Reid, P. J.; Keiding, S. R. *J. Am. Chem. Soc.* **2000**, *122*, 12795.

(33) Poulsen, J. A.; Thomsen, C. L.; Keiding, S. R.; Thogersen, J. *J. Chem. Phys.* **1998**, *108*, 8461.

(34) Thogersen, J.; Thomsen, C. L.; Poulsen, J. A.; Keiding, S. R. *J. Phys. Chem.* **1998**, *102*, 4186.

(35) Thogersen, J.; Jepsen, P. U.; Thomsen, C. L.; Poulsen, J. A.; Byberg, J. R.; Keiding, S. R. *J. Phys. Chem. A* **1997**, *101*, 3317.

(36) Philpott, M. P.; Hayes, S. C.; Thomsen, C. L.; Reid, P. J. *Chem. Phys.* **2001**, *263*, 389.

(37) Thomsen, C. L.; Philpott, M. P.; Hayes, S. C.; Reid, P. J. *J. Chem. Phys.* **2000**, *112*, 505.

(38) Hayes, S. C.; Philpott, M. P.; Mayer, S. G.; Reid, P. J. *J. Phys. Chem. A* **1999**, *103*, 5534.

(39) Hayes, S. C.; Philpott, M. J.; Reid, P. J. *J. Chem. Phys.* **1998**, *109*, 2596.

(40) Philpott, M. J.; Hayes, S. C.; Reid, P. J. *Chem. Phys.* **1998**, *236*, 207.

(41) Philpott, M. J.; Charalambous, S.; Reid, P. J. *Chem. Phys. Lett.* **1997**, *281*, 1.

(42) Fidder, H.; Tschirschwitz, F.; Dühr, O.; Nibbering, E. T. J. *J. Chem. Phys.* **2001**, *114*, 6781.

(43) Foster, C. E.; Barham, B. P.; Reid, P. J. *J. Chem. Phys.* **2001**, *114*, 8492.

(44) Salin, F.; Squier, J.; Mourou, G.; Vaillancourt, G. *Opt. Lett.* **1991**, *16*, 1964.

(45) Esposito, A.; Foster, C.; Beckman, R.; Reid, P. J. *J. Phys. Chem. A* **1997**, *101*, 5309.

(46) Press, W. H.; Flannery, B. P.; Teukolsky, S. A.; Vetterling, W. T. *Numerical Recipes in Pascal. The Art of Scientific Computing*; Cambridge University Press: Cambridge, 1992.

(47) Liu, C.-P.; Lai, L.-H.; Lee, Y.-Y.; Hung, S.-C.; Lee, Y.-P. *J. Chem. Phys.* **1998**, *109*, 978.

(48) Peterson, K. A.; Werner, H. J. *J. Chem. Phys.* **1996**, *105*, 9823.

(49) Delmdahl, R. F.; Baumgartel, S.; Gericke, K.-H. *J. Chem. Phys.* **1996**, *194*, 2883.

(50) The geminate-recombination yield in cyclohexane was calculated from ref 42. In that study, 57% of the OClO molecules in cyclohexane that dissociated to ClO were found to recombine. This, combined with the production quantum yield for ClO of ∼0.9 provides for a geminate-recombination yield of 0.50 ± 0.05. The geminate-recombination quantum yield in chloroform was determined from degenerate pump and probe studies at 390 nm, where only OClO and the Cl-solvent charge-transfer complex contribute to the optical-density evolution. The value of 0.26 ± 0.1 was calculated using a Cl production quantum yield of 0.1.

(51) Reid, P. J.; Esposito, A. P.; Foster, C. E.; Beckman, R. A. *J. Chem. Phys.* **1997**, *107*, 8262.

(52) Foster, C. E.; Reid, P. J. *J. Phys. Chem. A* **1998**, *102*, 3514.

(53) Delmdahl, R. F.; Bakker, B. L. G.; Parker, D. H. *J. Chem. Phys.* **2000**, *112*, 5298.

(54) Furlan, A.; Scheld, H. A.; Huber, J. R. *J. Chem. Phys.* **1997**, *106*, 6538.

(55) Coxon, J. A. *Can. J. Phys.* **1979**, *57*, 1538.

(56) McHale, J. L. *Molecular Spectroscopy*, 1st ed.; Prentice Hall: Upper Saddle River, New Jersey, 1999.

(57) Margulis, C. J.; Coker, D. F. *J. Chem. Phys.* **1999**, *110*, 5677.